Defense Technical Information Center Compilation Part Notice

ADP012187

TITLE: Characterization of the Order-Annealing Response of Nanostructured Iron-Palladium Based Ferromagnetic Thin-Films

DISTRIBUTION: Approved for public release, distribution unlimited

This paper is part of the following report:

TITLE: Nanophase and Nanocomposite Materials IV held in Boston, Massachusetts on November 26-29, 2001

To order the complete compilation report, use: ADA401575

The following component part numbers comprise the compilation report:
ADP012174 thru ADP012259

Mat. Res. Soc. Symp. Proc. Vol. 703 © 2002 Materials Research Society V3.4

Characterization of the order-annealing response of nanostructured iron-palladium based ferromagnetic thin-films

Huiping Xu[1)], Adam T. Wise[1)], Timothy J. Klemmer[2)] and Jörg M. K. Wiezorek [1)]

1) Department of Materials Science & Engineering, University of Pittsburgh, 848 Benedum Hall, Pittsburgh, PA 15261, USA;
2) Seagate Technology, 2403 Sidney Street, Pittsburgh, PA 15203, USA;

Abstract

A combination of XRD and TEM techniques have been used to characterize the response of room temperature magnetron sputtered Fe-Pd thin films on Si-susbtrates to post-deposition order-annealing at temperatures between 400-500°C. Deposition produced the disordered Fe-Pd phase with (111)-twinned grains approximately 18nm in size. Ordering occurred for annealing at 450°C and 500°C after 1.8ks, accompanied by grain growth (40-70nm). The ordered FePd grains contained (111)-twins rather than {101}-twins typical of bulk ordered FePd. The metallic overlayers and underlayers selected here produced detrimental dissolution (Pt into Fe-Pd phases) and precipitation reactions between Pd and the Si substrate.

Introduction

Tetragonal intermetallic phases, such as FePt, CoPt, MnAl and FePd, are of interest as active ferromagnetic materials in thermally stable high-information density thin film data storage media [1]. Due to their high magnetocrystalline anisotropy (~10^7-10^8 erg/cm^3) theoretical estimates predict thermally stable grain sizes resistant to spontaneous magnetization reversal in the range of approximately 3-5nm for these intermetallics [2]. Utilization of these intermetallic phases, which derive their attractive magnetic properties from their tetragonal ordered $L1_0$-type crystal structures with an easy magnetization axis parallel to the c-direction, promises up to about one order of magnitude increase in data storage densities with respect to current Co-based media.

Recent research on ferromagnetic intermetallic thin films for potential storage media applications focused mostly on FePt, CoPt and on property measurements, whereas relatively little published work on the structural evolution of FePd thin films during post-deposition treatments exists. FePd thin films have been grown successfully by molecular beam epitaxy (MBE) [3] and by magnetron sputtering on Pt-underlayers on MgO substrates [4]. The latter method allows more rapid deposition and is currently popularly employed in most industrial operations. Unlike MBE, magnetron sputtering without substrate heating usually produces intermetallic films that consist of the disordered solid solution rather than the ordered phases. In principle, substrate heating can be used to induce ordering during deposition but is usually accompanied by undesirable grain growth, producing less than optimal magnetization behavior [4]. Post-deposition annealing procedures that induce the ordering transformation offer potential control of the ordered phase grain size in room temperature sputtered Fe-Pd thin films. The development of optimized processing strategies for these nanostructured intermetallic materials systems, including potential alloying schemes, requires a basic understanding of the microstructural response of as-deposited Fe-Pd based thin films to annealing. Therefore, here exploratory studies have been performed of the microstructural response of magnetron sputtered Fe-Pd based thin films to post-deposition order-annealing. Combinations of X-ray diffraction (XRD) and imaging and analytical techniques of transmission electron microscopy (TEM) have been used in the characterization of the as-deposited and annealed films. Based on the experimental observations possible pathways for the evolution of the nanoscale microstructure are identified and discussed for the films studied here.

Experimental Procedure

FePd based thin films with nominal thickness of 100nm have been prepared by RF-magnetron sputtering at room temperature directly on Si substrates and on Si substrates with various metallic underlayers. Targets of an equiatomic Fe-Pd alloy together with high-purity elemental metal targets have been employed and all films were capped with a 5nm thick overlayer of Pt. Some pertinent parameters and compositions of deposited films are collated in table 1. Cleaved sections of the deposited films have been encapsulated in silica quartz tubes. The tubes have been evacuated down to ~10^{-3}torr and were then refilled with a reduced atmosphere of argon gas. Sequences of evacuation and argon refilling have been repeated three times before establishing a final partial pressure of ~$25x10^{-3}$ torr of argon in the tubes. The encapsulated films have been annealed isothermally at three different temperatures (400°C, 450°C and 500°C) for times between 1.8ks to 7.2ks. Plan-view and cross-sectional samples of the as-deposited and annealed films for transmission electron microscopy (TEM) have been prepared by standard methods. The structure of the films was characterized by a combination of X-ray diffraction (XRD) and TEM and scanning TEM (STEM) using Phillips X-pert diffractometers and a Jeol2000fx and a Tecnai F20, respectively. Compositional analyses of cross-sections have been performed by energy-dispersive X-ray spectroscopy (EDS) in the TEM and EDS-maps have been obtained by STEM.

Table I: Composition and dimensions of the magnetron sputtered FePd based thin films.

Sample ID	Overlayer	Active layer	Underlayer	Substrate
#810	Pt , 5nm	Fe-Pd, 100nm	Ti, 20nm	Si <100>
#811	Pt , 5nm	Fe-Pd, 100nm	NiCr, 15nm, Ta, 5nm	Si <100>
#813	Pt , 5nm	Fe-Pd, 100nm	none	Si <100>

Results

As-deposited thin films

Symmetric (θ/2θ)-XRD and glancing incidence scans for the three samples (for brevity not reproduced here) indicated that a significant <111>-fiber texture with the fiber-axis normal to the substrate developed in the active layers and that they consisted of the disordered fcc-phase γ-(Fe,Pd). The TEM analyses of the cross-sections of the as-deposited thin films confirmed the nominal compositions (spot-EDS) and desired dimensions for the various layers as summarized in table 1 (Fig. 1). Moreover, the γ-(Fe,Pd) layer exhibited a columnar morphology with about five individual grains of average grain size (18±4)nm constituting the columnar grains (Fig. 1). The individual γ-(Fe,Pd) grains exhibited profuse internal faulting (Fig. 1). Selected area and micro-diffraction (SAD and μD) together with bright field (BF) and dark field (DF) imaging tilting experiments have been used to determine that these faults are twins on {111}-planes parallel to the substrate/film interface (SAD in Fig. 1b). The SAD pattern (SADP) of Fig. 1b has been obtained from groups of columnar grains of similar orientations with <110>-zone axes approximately parallel to the electron beam. The twin-conjugation plane normal, $\mathbf{g}_{hkl}$=111, is marked by a solid white line and the open circles highlight some twin-reflections in Fig. 1b.

Annealed thin films

No structural changes were detected in XRD scans of the isothermally annealed samples (for brevity not reproduced here) for isothermal treatments at 400°C for up to 7.2ks. Structural changes associated with the annealing response of the Fe-Pd based thin films were observed for annealing at 450°C and at 500°C after 1.8ks. Apparent ordering of γ-(Fe,Pd) to γ_l-FePd, a loss of

Pt and the formation of additional phases could be inferred qualitatively from the XRD data. TEM imaging and diffraction analyses of cross-sections of the annealed films have been performed and a number of microstructural changes have been identified. The TEM observations confirmed that the active layer ordered to γ_1-FePd with the tetragonal $L1_0$-structure (Fig. 2 & 3). The ordered FePd grains exhibited twinning on {111} (Fig. 2b). Furthermore, the local loss of the Pt-overlayer has been observed (Fig. 2). In regions that retained the Pt-overlayer the active layer exhibited a columnar grain structure with the increased average grain size of approximately 40-70nm (Fig. 2,3). PdSi precipitates of up to about 250nm in size formed periodically at the film/substrate interface and consistently in regions of the film where the Pt-overlayer had disintegrated (Fig. 2, 3). The PdSi precipitates have been characterized by EDS, SAD and μD. These buried precipitates exhibited an approximately equiatomic composition, $Pd_{48}Si_{52}$ (all in mol%), and their structure was determined to be consistent with an ordered orthorhombic MnP-type structure (Pnma) with a_0=5.617Å, b_0=3.391Å and c_0=6.153Å [5]. The additional peaks observed in the XRD scans for some of the annealed samples that were not associated with FePd, Pt, Ti and Si could be indexed consistent with respect to the orthorhombic PdSi phase. The ordered γ_1-FePd grains that formed in the vicinity of the buried PdSi precipitates also exhibited internal twining on {111} but the columnar grain morphology of the active layer was largely lost (Fig. 3). The composition of these latter γ_1-phase grains (Fig. 3) was determined by EDS to be $Fe_{53}Pd_{36}Pt_{11}$ (in mol%). Hence, significant amounts of Pt, dissolved into the γ_1-phase matrix, which may be described as approximately equiatomic in composition with respect to the ratio of Fe to (Pd + Pt). EDS mapping by STEM has been utilized to analyze the area depicted in Fig. 3, allowing a correlation of element distributions in the annealed film. Comparison of the STEM BF image and elemental O- and Fe-maps (Fig. 4) reveals a strong correlation between the spatial distribution of oxygen and Fe. The regions that exhibited significant correlation between strong enrichment in O and Fe have been labeled Fe_xO_y in Fig. 2 and 3. Hence, it appears reasonable to conclude that interspersed with the γ_1-phase grains Fe-based oxides formed in regions where the Pt-overlayer disintegrated in response to the isothermal annealing (Fig. 2-4). Such oxide formation was not detected in the regions with columnar γ_1-FePd and intact Pt-overlayer. However, the EDS analyses of these latter regions indicated significant enrichment of the Ti-underlayer with Pd (e.g. Fig. 2, label Ti-Pd).

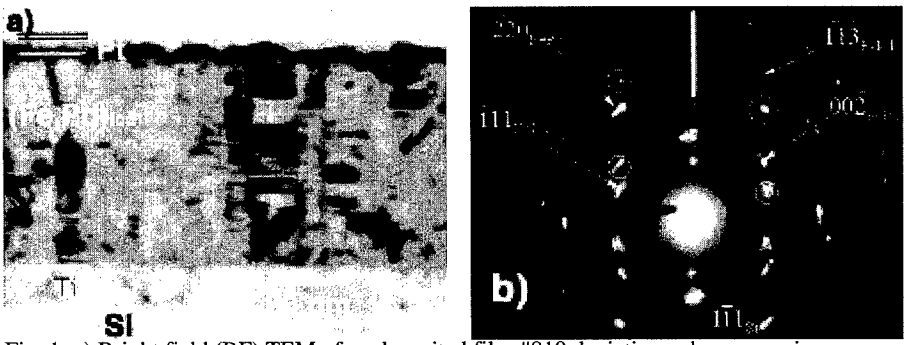

Fig. 1: a) Bright field (BF) TEM of as-deposited film #810 depicting columnar grain morphology. b) selected area diffraction pattern (SADP) from strongly diffraction region, approximately in center of a), for BD ~ <110> of g-(Fe,Pd); open circles mark (111)-twin spots and white line marks direction of conjugation plane normal.

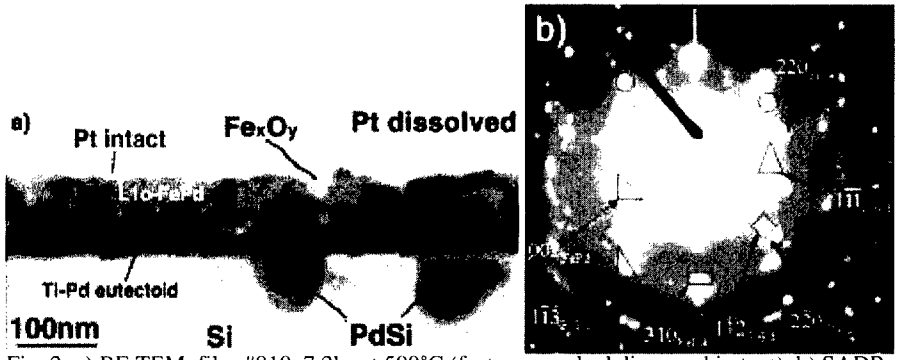

Fig. 2: a) BF-TEM, film #810, 7.2ks at 500°C (features marked discussed in text). b) SADP from region $L1_0$-FePd in a) for approximate beam direction (BD) of [110]; open circles mark (111)-twin spots, triangles and rectangles mark superstructure spots from γ_1-FePd.

DISCUSSION

Room temperature magnetron sputtering of Fe-Pd films on Si-substrates and under the conditions employed here produces an active layer with columnar morphology comprised entirely of disordered γ-(Fe,Pd) grains, which are profusely twinned on (111) parallel to the film/substrate interface plane and on average approximately 18nm in diameter. In response to isothermal annealing at 400°C for up to 7.2ks no microstructural changes were detected by XRD. Annealing at the higher temperatures of 450°C and 500°C for times as short as 1.8ks induced the transformation of the disordered γ-(Fe,Pd) phase to $L1_0$-ordered γ_1-FePd in the active layer. The ordering of the Fe-Pd phase was accompanied by significant grain growth, producing elongated grains with their largest dimension normal to the film and with maximum diameters in the range of 40-70nm. The typically about five disordered grains that comprised the columnar grains in the as-deposited films are usually separated by low-angle grain boundaries (LAGB). It appears reasonable to propose that some of these LAGB have been eliminated and adjacent prior γ-(Fe,Pd) grains in a column of grains coalesced to form the larger elongated grains of the ordered phase during annealing. The transformation from the disordered phase to the ordered phase is associated with a volume change of approximately 1.7% and a reduction in symmetry of the crystal structure. Hence, in order to minimize the attendant transformation strains the characteristic polytwin structures with dodecahedral {101}-twin conjugation develop during the ordering process in bulk samples of γ_1-FePd [6]. Interestingly, the ordered γ_1-FePd grains in the annealed thin films studied here retained a large density of the octahedral (111)-conjugated twins. Presumably, these (111)-twins have been inherited from the disordered phase. Dodecahedral {101}-twins, characteristic of γ_1-FePd bulk samples [6], have not been observed. Hence, it is tempting to speculate that a critical grain size exists for the γ_1-FePd phase below which the transformation strain

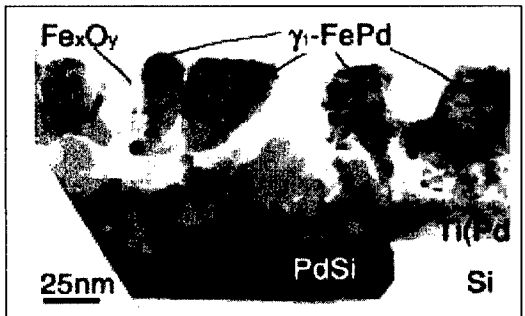

Fig. 3: Film #810, annelaed for 7.2ks at 500°C. BF TEM of region in vicinity of PdSi precipitate at film/substrate interface. See text for details

induced {101}-conjugated twins do not form during isothermal annealing. The additional degree of freedom afforded by the thin film geometry as compared with bulk samples may influence such a scaling effect in the microstructural response to isothermal ordering. The observation regarding the twin fault plane is interesting, because the nature of the defect structures in the ordered phase is predicted to significantly affects magnetic hysteresis behavior and requires further investigation.

In addition to the desirable ordering transformation a number of undesirable microstructural changes were detected. Intermetallic precipitates of an orthorhombic PdSi phase formed periodically at the film/substrate interface. Pd from the active layer grains diffused into the Ti-underlayer. The Pt-overlayer locally dissolved and Pt was incorporated as a solute into the γ_1-phase grains. The consistent correlation between local loss of the Pt-overlayer and formation of the buried PdSi precipitates may be indicative of some synergism between the inward (toward the substrate) diffusion of Pt and Pd. The γ_1-FePd grains in the active layer above the PdSi precipitates have an approximately equiatomic composition with respect to the ratio of Fe to the sum of Pd plus Pt. This is consistent with Pt atoms from the dissolving Pt-overlayer migrating into the active layer forming solute species in the Fe-Pd grains. The polycrystalline Pt-overlayer was only one grain thick and GB's exhibited considerable local curvature and signs of surface grooving prior to annealing (Fig. 1a). With thermal activation during annealing a driving force exists to initiate the inward diffusion of Pt into the active layer from these curved and grooved GB's. Hence, it appears reasonable to propose that the local decomposition of the Pt-overlayer involved diffusion of Pt, preferentially from grooved GB's in the overlayer, along the boundaries between the columns of grains in the active layer, followed by irrigation of the LAGB between individual Fe-Pd grains in adjacent columns. Once the Pt reached the LAGB's between individual active layer grains, incorporation into the lattices of the ordering γ-phase and/or the already ordered γ_1-phase would require bulk diffusion. The buried PdSi precipitates grew into the Si-substrate (Fig. 2,3). Thus, diffusion of Pd from the active layer through the underlayer into the substrate occurred. At a temperature of 760°C a eutectic of Pd and Pd_3Si exists in the Si-Pd binary system. Neither of these phases has been observed in the films studied here, which is not surprising, since annealing was performed well below the eutectic temperature. However, considering a solid-state reaction between Pd and Si that starts with a Si-rich composition and if Pd is the faster diffusing species, the binary phase diagram indicates that at temperatures at or below 500°C the line compound PdSi would be predicted. Hence, the observed growth morphology, crystal structure and composition of the intermetallic PdSi precipitates at the film/substrate interface is consistent with the Si-Pd phase diagram. Based on the phase diagram of the Ti-Pd binary system, at or below 500°C solid state diffusion of Pd into the Ti-underlayer could potentially produce eutectoid mixtures of Ti, Ti_4Pd and Ti_2Pd, depending on the local Pd

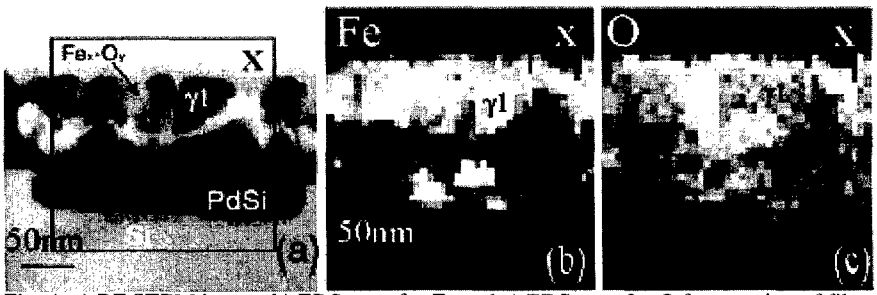

Fig. 4: a) BF STEM image, b) EDS-map for Fe and c) EDS map for O from region of film #810 shown in Fig. 3. The X marks identical positions in each figure, b) and c) have the same scale, γ_1 marks an ordered FePd grain and Fe_xO_y marks Fe-based oxide.

composition. Interestingly, Pd enrichment of the Ti underlayer was detected by EDS analyses in the regions between the buried PdSi precipitates (label in Fig. 2). Thus, Pd diffused into the underlayer and eutectoid Ti-Pd mixtures would form prior to PdSi precipitates. The Pd diffusion into and through the Ti layer is a required intermediate step in the formation of the PdSi phase, which locally lead to disintegration of the Ti-underlayer. Gaseous species, such as O, present in the residual Ar-based atmosphere of the silica-quartz tubes during annealing also diffused into the film. This process was rapid after the protective Pt-overlayer locally disintegrated resulting in Fe-oxides near the PdSi precipitates. PdSi precipitation depleted adjacent active layer grains of Pd, rendering them less precious and less oxidation resistant. Observation of the Fe-oxides in the regions with disintegrated Pt-overlayer and buried PdSi precipitates is consistent with the oxidation of the Pd-depleted active layer grains (Fig. 3,4). Similar observation to those presented here for film #810 have been made for the other films. The undesirable microstructural changes reported here are attributed to the interplay of the solid-state reactions between Pt-metal atoms and the Fe-Pd based phases and between Pd and the chosen metal-underlayers and Si-substrate respectively, together with the residual oxygen partial pressure present in the annealing environment. Ti and NiCr are unsuitable diffusion barriers to prevent detrimental reactions between Pd and Si. Pt is unsuitable as an overlayer for Fe-Pd based active layers.

CONCLUSIONS

A combination of XRD and TEM techniques have been used to characterize the response of room temperature magnetron sputtered Fe-Pd thin films on Si susbtrates to post-deposition order-annealing. The main conclusions of this preliminary study can be summarized as follows:

- As-deposited active layers consist of the disordered phase with (111)-twinned grains approximately 18nm in size.
- The Fe-Pd orders upon annealing in excess of 1.8ks at 450°C and 500°C.
- Ordered FePd grains in annealed films grew to maximum dimensions of 40-70nm and exhibit (111)-twins. Dodecahedral {101}-twins typical of the ordered FePd in the bulk were not observed.
- Pt dissolves into Fe-Pd phases and is unsuitable as an overlayer.
- The metallic underlayers were unsuitable to prevent detrimental precipitation reactions between Pd and the Si substrate.
- Post-deposition treatments of room temperature sputtered films are susceptible to local oxidation and thus should be performed in ultra-high vacuum or otherwise controlled inert atmospheres.

ACKNOWLEDGMENTS

The authors thank the Office of Research of the University of Pittsburgh, Small Grants Program, Central Research Development Fund, and Seagate Technology for financial support of this study, and Tom Nuhfer, Department of Materials Science and Engineering, Carnegie-Mellon University, for assistance with the EDS mapping by STEM.

REFERENCES

[1] T.J. Klemmer, D. Hoydick, H. Okumura, B. Zhang, W.A. Soffa, Scripta Metall. **33**, 1793 (1995).
[2] D. Weller, A. Moser, IEEE Trans. Magn., **35**, 4423 (1999).
[3] P.R. Aitchison, J.N. Chapman, V. Gehanno, I.S. Weir, M.R. Scheinfein, S. McVitie, A. Marty, J. Magn. Magn. Mat., **223**, 138 (2001).
[4] A. Cebollada, P. Caro, J.L. Menendez, F. Briones, D. Garcia, A. Hernando, J.A. Garcia-Diaz, J. Magn. Mat., **203**, 162 (1999).
[5] J.H. Westbrook, *Intermetallic Compounds*, (Robert E. Krieger Publishing Co., Huntington, NY, 1977).
[6] B. Zhang, M. Lelovic, W.A. Soffa, Scripta Metall. **25**, 1577 (1991).